

Topical Perspectives

The mechanisms of gallium-catalysed skeletal rearrangement of 1,6-enynes – Insights from quantum mechanical computations

Joseph Bortey Borketey, Ernest Opoku, Richard Tia*, Evans Adei

Theoretical and Computational Chemistry Laboratory, Department of Chemistry, Kwame Nkrumah University of Science and Technology, Kumasi, Ghana

ARTICLE INFO

Article history:

Received 28 August 2019

Received in revised form

4 October 2019

Accepted 7 October 2019

Available online 10 October 2019

Keywords:

Skeletal reorganization

1,6-Enynes

Gallium catalysis

Cycloisomerization

Post-transition metal

Mechanistic study

ABSTRACT

The transition metal-catalysed skeletal reorganization of 1,6-enynes can lead to three types of products – a type **I** product occurring via the cleavage of the alkene C–C bonds and the migration of the terminal alkene carbon to the terminus of the alkyne; a type **II** product arising from cleavage of both the double and the triple bonds followed by insertion of the terminal alkene carbon into the alkyne C–C triple bond; and a type **III** product which is obtained when there is a cleavage of the olefinic bond followed by formation of two new bonds from each carbon to each of the acetylenic carbons. The course of these reactions is highly dependent on the metal catalyst used and type of substitution at the alkene and alkyne moieties of the enyne. In this mechanistic study of the re-organization of 1,6-enynes catalysed by GaCl₃, performed at the DFT M06/6-311G(d,p) level of theory, the parent reaction selectively leads to the formation of the type **I** product through the formation of the open cyclopropane ring. The presence of substituents at the acetylenic moiety governs the preferred position of the metal along the alkyne bond within the pi-complex: with electron-withdrawing groups (EWGs), the metal prefers the terminal carbon while electron-donating groups (EDGs) lead to the metal preferring the internal carbon. EWGs at the alkyne moiety efficiently favour the formation of the type **I** product. Substituents at the olefin moiety alter the mechanism of the reaction which may favour the selective formation of the type **I** or **III** product depending on the type of substituent. EWGs at the olefinic moiety favour formation of the type **III** product when the alkyne moiety is unsubstituted while EDGs forms the type **I** product selectively. Solvent and temperature have no substantial effects on the energetic trends and product distribution. Hence, gas-phase calculations are deemed adequate for the problem at hand.

© 2019 Elsevier Inc. All rights reserved.

1. Introduction

Enynes are an interesting class of molecules as they possess both the alkene and alkyne functionalities, increasing the diversity of reactions they undergo. Cycloisomerisation of 1,n-enynes is a powerful approach for the syntheses of a large variety of products depending on the type of metal catalyst used as well as the functionalized starting material employed [1–4]. The electrophilic activation of alkynes by transition metal halides or their cation complexes, such as Ru(II), Pt(II), Au(I), and even typical elemental halides, such as Ga(III) and In(III), has been recognized as a key step in various cycloisomerization reactions of alkyne derivatives, such as enynes [5–9]. Cycloisomerization of 1,n-enynes can either

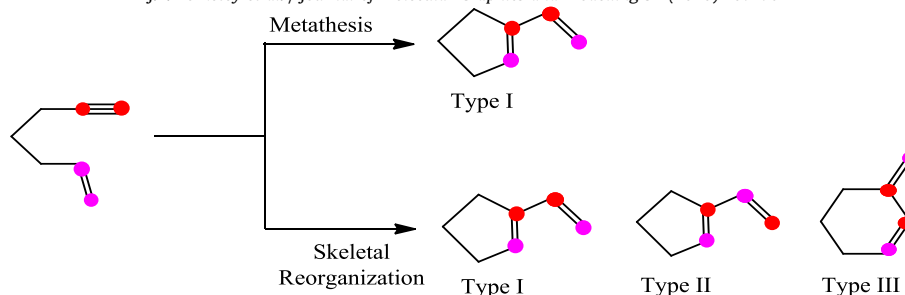
proceed through metathesis or skeletal reorganization. The mechanism for enyne metathesis selectively leads to formation of the type **I** products in which the original acetylenic carbons remain connected consecutively (Scheme 1) [10–12].

The skeletal reorganization of enynes which leads to 1-vinylcycloalkenes can lead to three possible products, types **I** and **II**, and **III** products (Scheme 1). The formation of type **I** product involves the cleavage of the alkene C–C bonds and the migration of the terminal alkene carbon on the terminus of the alkyne. The type **II** product, however, involves cleavage of both the C–C double and C–C triple bonds. The terminal alkene carbon migrates between the two alkyne carbons. The type **III** product is obtained when there is a cleavage of the olefinic bond and two new bonds are formed from each carbon to each of the acetylenic carbons [9,13,14]. The course of these reactions is highly dependent on the metal catalyst used and type of substitution at the alkene and alkyne moiety of the substrate.

Enyne skeletal rearrangement serves as very important

* Corresponding author.

E-mail addresses: jborketeybortey@gmail.com (J.B. Borketey), ernopoku@gmail.com (E. Opoku), richtiagh@yahoo.com (R. Tia), eadei@yahoo.com (E. Adei).



Scheme 1. Transformation of enynes to their conjugated dienes.

transformation because of the ease in obtaining the functionalized starting materials as well as the numerous cyclic derivatives that can be obtained when different experimental conditions and different functionalized starting materials are employed (Scheme 2) [15]. These attributes make the metal-catalysed process atom-economical and simple to perform on large scale.

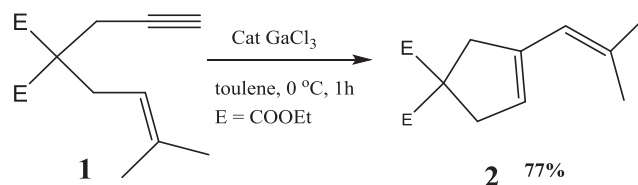
The first enyne skeletal reorganization was performed using Pd (II) complex to expand the utility of transition metal-catalysed alkylation which lead to the formation of the closed five-membered ring di-ene (**g**) as well as other cycloadducts [3].

In other related studies, simple metal halides such as $[\text{RuCl}_2(\text{CO})_2]_2$ have been established to show a high catalytic activity for the skeletal reorganization of enynes having a terminal acetylenic moiety leading to type I product [6].

The use of GaCl_3 catalyst in the cycloisomerization of ω -aryl-1-alkyne has been shown to improve the reaction significantly compared to previously reported catalytic systems [16]. The first gallium-catalysed enyne skeletal reorganization reported was limited to alkyl substituents at the olefinic moiety only [8]. These reactions which include the reaction of 1,6 enyne **1** with a catalytic amount of GaCl_3 (1 M in a methylcyclohexane solution) in toluene at 0°C offered a yield of about 77% of the type I product within 1 h (Scheme 3).

The skeletal reorganization of enynes with GaCl_3 bearing two substituents at the olefinic terminal carbon undergo an efficient skeletal reorganization, and enynes that are mono-substituted at the terminal olefinic carbon undergo a stereospecific skeletal reorganization with respect to the geometry of the olefin moiety (Scheme 4).

In explaining the stereospecific skeletal reorganization with respect to the geometry of substituents at the olefin moiety, a



Scheme 3. Skeletal reorganization of enyne **1** to yield product **2**.

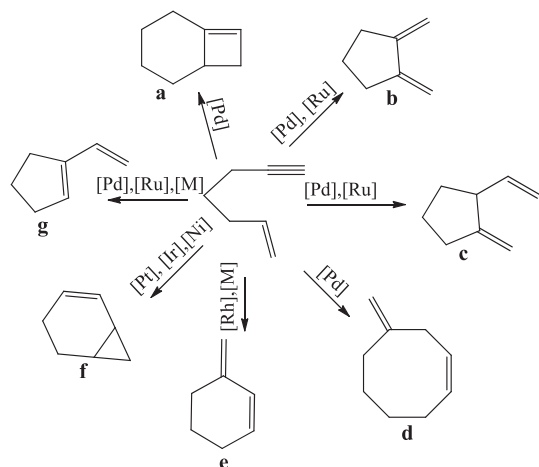
computational study at the DFT B3LYP/6-31G* level of theory revealed that the reaction proceed through the formation of an open cyclopropane ring [17]. It should be noted that this computational study by Xu et al. [17] proposing the 3c-2e cyclopropane mechanism was limited to only a methyl substitute at the olefin moiety.

Application of computational chemistry techniques in catalysis and reaction mechanisms continue to play a dominant role in contemporary chemistry as evident in selected studies on computational catalysis [18–20]. In view of the fact that the product outcomes of the metal-catalysed skeletal reorganization of 1,6-enynes is highly sensitive to the type of substituent on both the olefinic and acetylenic moieties, it is important to study the mechanism of this important reaction by considering substituents beyond the methyl substituent at the olefinic position. Therefore, a thorough mechanistic study is a necessity to augment the existing literature. In addition, effects of temperature and solvent on energetic trends in this present reaction would be important to provide guidance for correlative experiments. This work therefore reports a detailed exploration of the potential energy surface of the skeletal reorganization of the parent 1,6-enynes, with particular emphasis on the effects of substituents at both the olefinic and acetylenic moieties on product distribution. In addition, effects of solvent and temperature on energetic trends are also investigated. These mechanistic concerns/issues will be answered as outlined in Scheme 5.

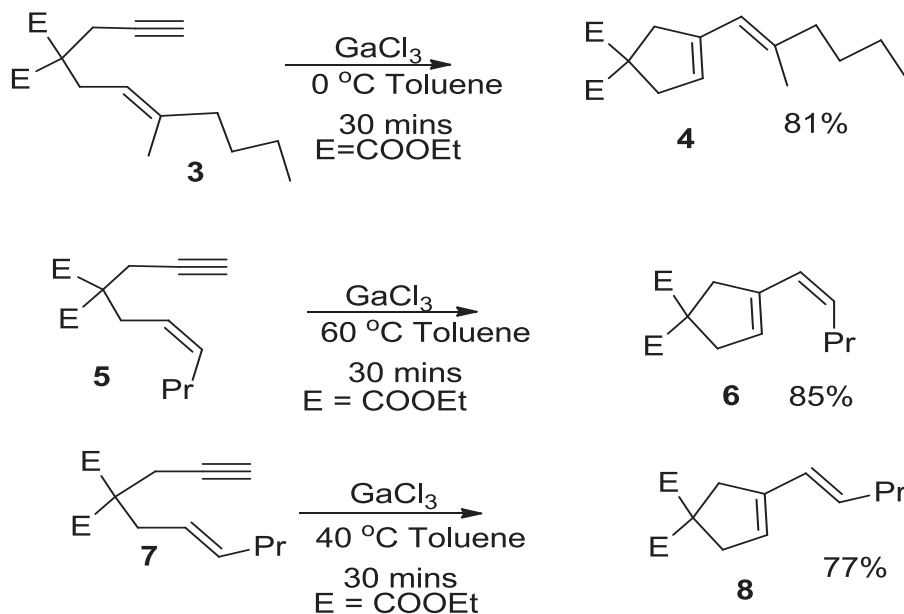
2. Computational details and methodology

All the quantum mechanical calculations were performed using the Spartan'14 [21] and Gaussian 09 [22] Molecular Modeling software suites at the M06/6-311G(d,p) level of theory. The M06 functional developed by Zhao and Truhlar [23] is a hybrid meta-gradient-corrected functional (meta-GGA) with 27% of the Hartree-Fock exchange term established to be effective at computing thermochemical and kinetic parameters especially where nonlocal dispersion interactions play a dominant role [24]. Using the polarizable continuum model (PCM), toluene was employed to compute solvation effects in the reactions [25].

The initial geometries of the structures were built using Spartan's graphical model builder and minimized interactively using



Scheme 2. Cycloisomerization of enynes to form different products using various metal catalysts. $[\text{M}] = [\text{Ga}]$ or $[\text{In}]$.



Scheme 4. Skeletal reorganization of enyne leading to type I products as reported by Chatani et al. [8].

the sybyl force field [26]. Transition state structures were computed by first obtaining guess input structures. This was done by constraining specific internal coordinates of the molecules (bond lengths, bond angles, dihedral angles) while fully optimizing the remaining internal coordinates. This procedure offers appropriate guess transition state input geometries which are then submitted for full transition state calculations without any geometry or symmetry constraints. Full harmonic vibrational frequency calculations were carried out to ensure that each transition state structure had a Hessian matrix with only a single negative eigen value, characterised by an imaginary vibrational frequency along the respective reaction coordinates. Intrinsic reaction coordinate calculations were then performed to ensure that each transition state smoothly connects the reactants and products along the reaction coordinate [27–32]. The full optimization of all structures were carried out with the Gaussian 09 [22] computational chemistry software. The default self-consistency field (SCF) convergence criteria (SCF=Tight) within the Gaussian 09 molecular modeling package was used for all the computations [33,34].

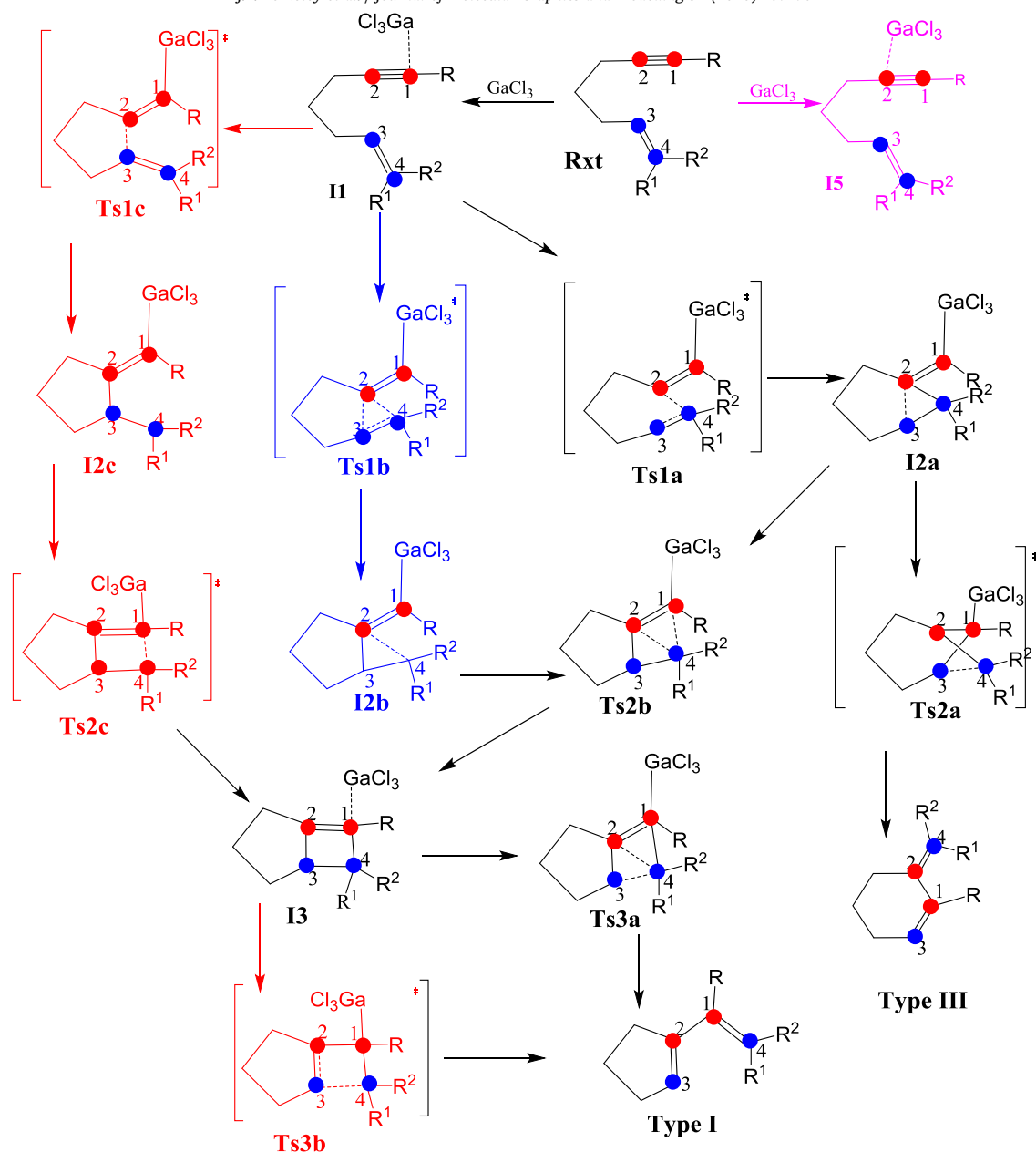
3. Results and discussions

3.1. Mechanism of the skeletal reorganization of the parent enyne

The optimized geometries of the reactants, transition states and intermediates and the Gibbs free energy profile of the GaCl_3 -catalysed skeletal reorganization of the parent enyne (1,6-enyne) are shown in Fig. 1. The proposed mechanism for the skeletal reorganization is shown in Scheme 5. The GaCl_3 -catalysed skeletal reorganization of the parent 1,6-enyne takes place along the three-membered structure containing the cyclopropane ring (**Ts2b**) which leads to the formation of the type I product selectively.

In this pathway, the first step involves the formation of a pi-complex intermediate between GaCl_3 and the C1–C2 bond of the alkyne moiety to generate **I1** with the GaCl_3 displaced towards C1. **I1** has a relative energy of -24.3 kcal/mol. The slight increase in the triple bond length from 1.21 Å in the reactant to 1.23 Å in the complex is as a result of the weakening of the C1–C2 triple bond due to the complexation. The C1–Ga and C2–Ga bond lengths are

2.25 Å and 2.59 Å respectively. **I1** rearranges through **Ts1a** to form **I2**. Due to the electron withdrawing nature of GaCl_3 , the C2 carbon becomes more electron deficient. Simultaneously there is an electron density flux to the C2 carbon in **Ts1a** forming the unclosed cyclopropane ring in **I2a**. This takes place through an energy barrier of 10.0 kcal/mol. At the transition state, C1–C2 bond loses more of its triple bond character, increasing from 1.28 Å to 1.37 Å which is the length of a typical C–C double bond. The Ga–C1 bond shortens from 2.07 Å in **Ts1a** to 2.02 Å in **I2** indicating formation of a full Ga–C1 bond. The C2–C3 and C2–C4 bond further closes from 2.31 Å and 2.22 Å in **Ts1a** to 1.70 Å and 1.56 Å in **I2a** respectively showing the partial formation of a single bond along C2–C3 and a single bond along C2–C4. The C3–C4 partially loses its double bond character, increasing from 1.35 Å in **Ts1a** to 1.43 Å. The C2–C3–C4 in **I2a** indicate a three-centre two-electron (3c–2e) bond which is transferred to C1–C2–C4 in **Ts2b** to generate **I3**. The formation of the 3c–2e bond in **I2a** and **Ts2b** is consistent with the mechanism proposed by Xu et al. [17]. The intermediate **I2a** is found to proceed with very low barrier towards rearrangement (1–2 kcal/mol) as seen in Fig. 1 is therefore expected to have a very short lifetime. The activation barrier for this step is 2.0 kcal/mol producing **I3** with relative energy of -47.3 kcal/mol. The elementary step through **Ts2a** leading to the formation of the type III product with relative energy of -66.1 kcal/mol is less favoured by 1.8 kcal/mol. In **Ts2a**, the C1–C2 elongates and from 1.37 Å to 1.59 Å. The C3–C4 bond breaks and elongates to 2.03 Å while double bond start forming along C2–C4. In all, **Ts2a** transforms to **Pdt2** which is the type III product. The C1–C3 and C2–C4 bond length are 1.37 Å and 1.34 Å. In **Ts2b**, a new single bond is formed between C1 and C4 with a bond length of 2.41 Å. The C1–C2 bond length remains fairly constant while the C2–C3 bond shortens from 1.58 Å to 1.51 Å. In **I3** the GaCl_3 is weakly coordinated before going through **Ts3** with activation barrier of 14.6 kcal/mol to form **Pdt1** with relative energy of -60.6 kcal/mol. The C1–C4 and C2–C3 bond lengths are 1.38 Å and 1.35 Å. The Ga–C1 bond in **Pdt1** and **Pdt2** is 2.63 Å and 2.51 Å respectively. The type I (**Pdt1**) product is selectively formed. Again, the selective formation of the type I product is consistent with the work of Chatani et al. [8], and the proposed mechanism by Xu et al. [17].



Scheme 5. Proposed scheme of study for the mechanism of the skeletal reorganization of 1,6 enynes using GaCl_3 .

The various transition states **Ts1a**, **Ts2a**, **Ts2b** and **Ts3** are each characterised by a single imaginary frequency for each transition structure, $303.5i \text{ cm}^{-1}$, $260.9i \text{ cm}^{-1}$, $46i \text{ cm}^{-1}$ and $138.5i \text{ cm}^{-1}$ respectively. **Ts1a** occurs through the vibration of C2 relative to the C3–C4 bond giving rise to the 3c–2e bond. In **Ts2a** the vibration is along the C3–C4 bond. **Ts3b** vibrate along the C1 – C4. **Ts3** vibrates along the C3 – C4 bond.

3.2. Effects of substituents on the mechanism of the skeletal reorganization

We employed various electron-withdrawing groups (EWGs) and electron-donating groups (EDGs) as substituents at the acetylenic moiety to investigate the effects on the mechanism of the reaction (see Table 1). When EWGs such as $-\text{Cl}$, $-\text{CN}$, $-\text{NO}_2$, and $-\text{COOCH}_3$ were employed, the reaction consistently follows the parent

mechanism with the metal sitting on C1 carbon in the pi-complex **II**. We also employed EDGs such as $-\text{NH}_2$, $-\text{OH}$, $-\text{Ph}$, as well as various alkyl substituents. The alkyl substituents also have the metal sitting on the C1 and will go through the parent mechanism. The stronger EDGs (Ph , NH_2 , and OH) have the metal sitting on the C2 carbon which can rearrange to form **I5** as shown in Scheme 5. We can now account that substituent at the acetylenic moiety governs the position of the GaCl_3 along the C1–C2 alkyne bond and that all EWGs and alkyl groups have the metal sitting on the C1 carbon. The stronger EDGs have the metal sit on the C2 along the C1–C2 triple bond. For purposes of brevity, the optimized geometries of some selected structures are shown in Fig. 2.

Substituents at the olefinic moiety are oriented along the C3–C4 plane and control the coordinate along which the reaction proceeds to determine the products formed. Presence of EWGs at the olefinic moiety favour the formation of the type III product.

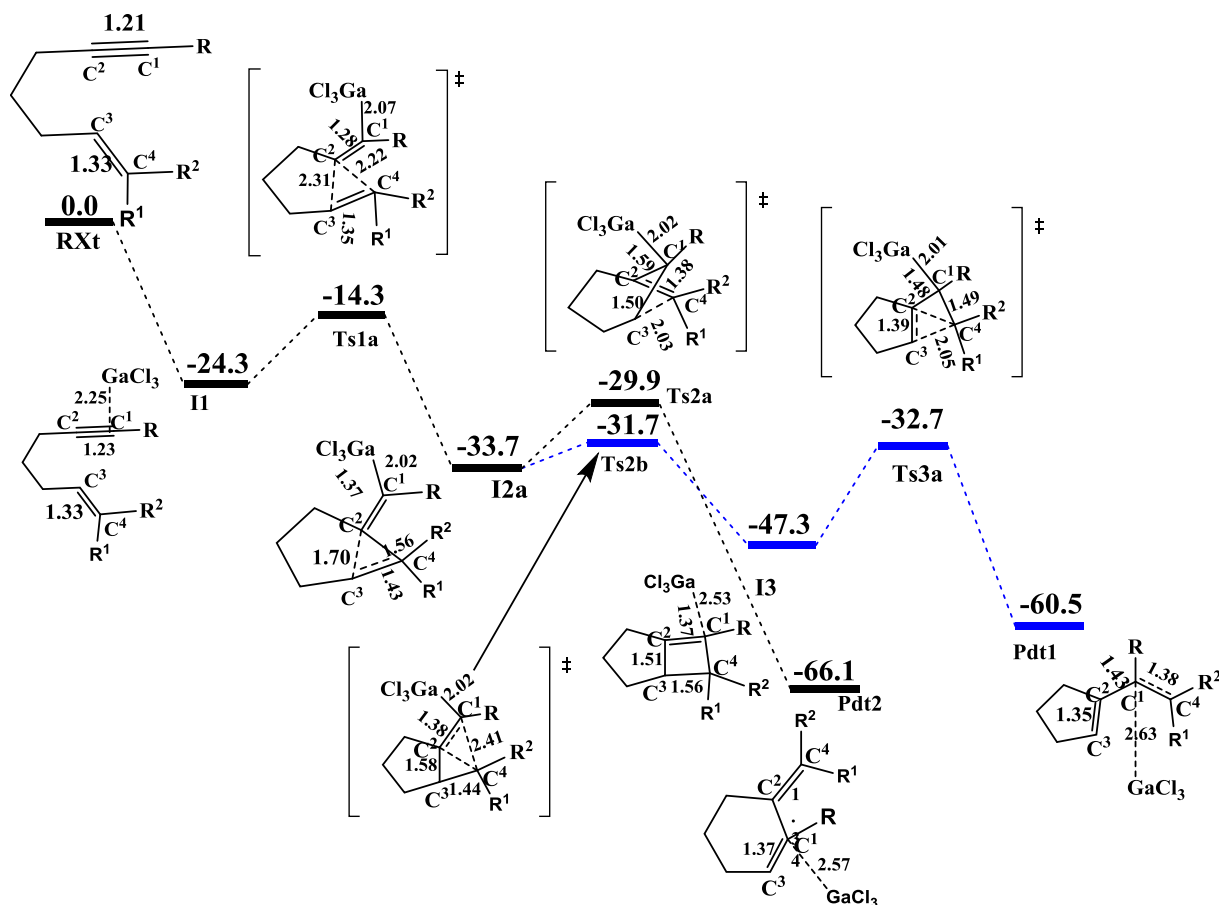


Fig. 1. Gibbs free energy profile of the skeletal reorganization of the parent enyne at the M06 level and 6-311G(d,p) basis set. Relative energies in kcal/mol. All bond distances are measured in Å. $R = R^1 = R^2 = H$.

Table 1

Relative energies of the stationary points on the potential energy surface, reaction energies and activation barriers for the substituted enynes at the acetylenic moiety. All energies are measured in kcal/mol.

R	I1	Ts1a	I2	Ts2a	Ts2b	I3	Ts3a	Pdt1	Pdt2	Ea1	Ea2a	Ea2b	Ea3
H	-24.3	-14.3	-33.7	-29.9	-31.7	-47.3	-32.7	-60.6	-66.1	10.0	3.8	2.0	14.6
Cl	-20.8	-13.9	-44.4	-30.5	-41.2	-43.0	-36.0	-66.4	-68.2	6.9	13.9	3.2	7.0
CN	-14.6	-10.6	-28.8	-19.7	-26.0	-39.7	-26.5	-49.8	-55.1	4.0	8.6	2.3	13.5
COOCH ₃	-27.7	-18.1	-40.7	-29.2	-39.2	-54.3	-35.6	-61.7	-67.4	9.6	11.5	1.5	18.7
NO ₂	-14.4	-14.0	-43.8	-37.6	-41.0	-47.8	-42.9	-64.4	-67.2	0.4	6.2	2.8	4.9

Ea1 is the first barrier leading to the formation of I2. Ea2a and Ea2b are the activation barrier leading to the formation of the Type III and I3 respectively. Ea3 is the last elementary step leading to formation of the Type I product.

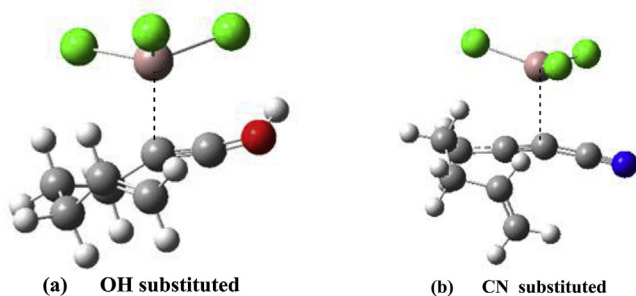


Fig. 2. Optimized geometries of selected pi-complexes showing substitution effect at the acetylenic moiety on the position of GaCl₃ on the enyne.

We employed the EWGs and EDGs mono-substituted enynes at the cis conformer as well as di-substituted enynes at the olefin moiety. In all, the substituents are oriented along the C3–C4 plane. When strong EWGs are employed, **Ts1b** formed with vibration occurring along the C2–C4. When mono substituted weak EWGs are employed, the vibration occurs along the C2 relative to the C3–C4 bond. Di-substituted weak EWGs forms **Ts1c** with the vibration occurring along the C2–C3 bond. All the EWGs form **I2a** which is the key intermediate leading to the formation of the type III product. All the other transition states, **Ts2a**, **Ts2b**, **Ts3** occurring between the same carbons as observed in the parent.

All di-substituted EDGs have their first transition state **Ts1c** occurring along the C2–C3 leading to the formation **I2b** and **I2c** (Scheme 5). Formation of **I2b** and **I2c** selectively reorganizes to form the type I product. **I2a** is formed when mono-substituted weak alkyl groups are employed. **I2b** is formed instead when

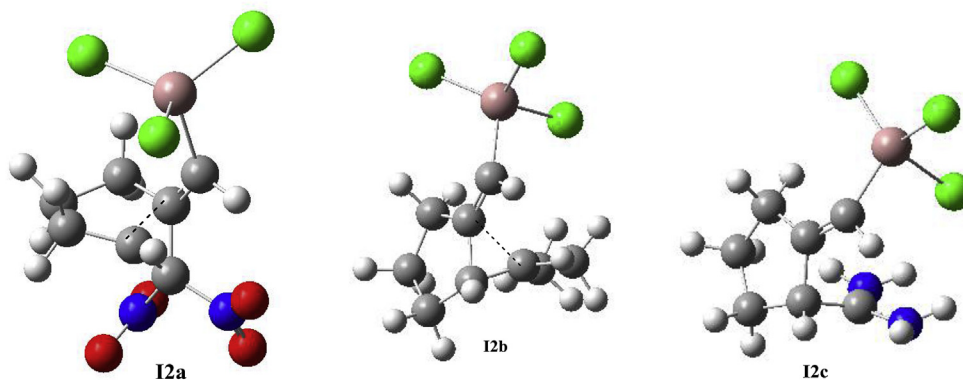


Fig. 3. Optimized geometries showing the main intermediate favouring the formation of the type I and III product.

long chains alkyl groups are employed (Fig. 3). This explains the high selectivity of the type I product with increasing alkyl chains as reported by Chatani et al. [8]. The **I2a** formation pathway is

preferred when the methyl group (smallest alkyl chain) is employed. The stronger EDGs such as $-\text{NH}_2$ and $-\text{OH}$ form the type I product through **Ts2c** and **Ts3b** rather than **Ts2b** and **Ts3a**. Except

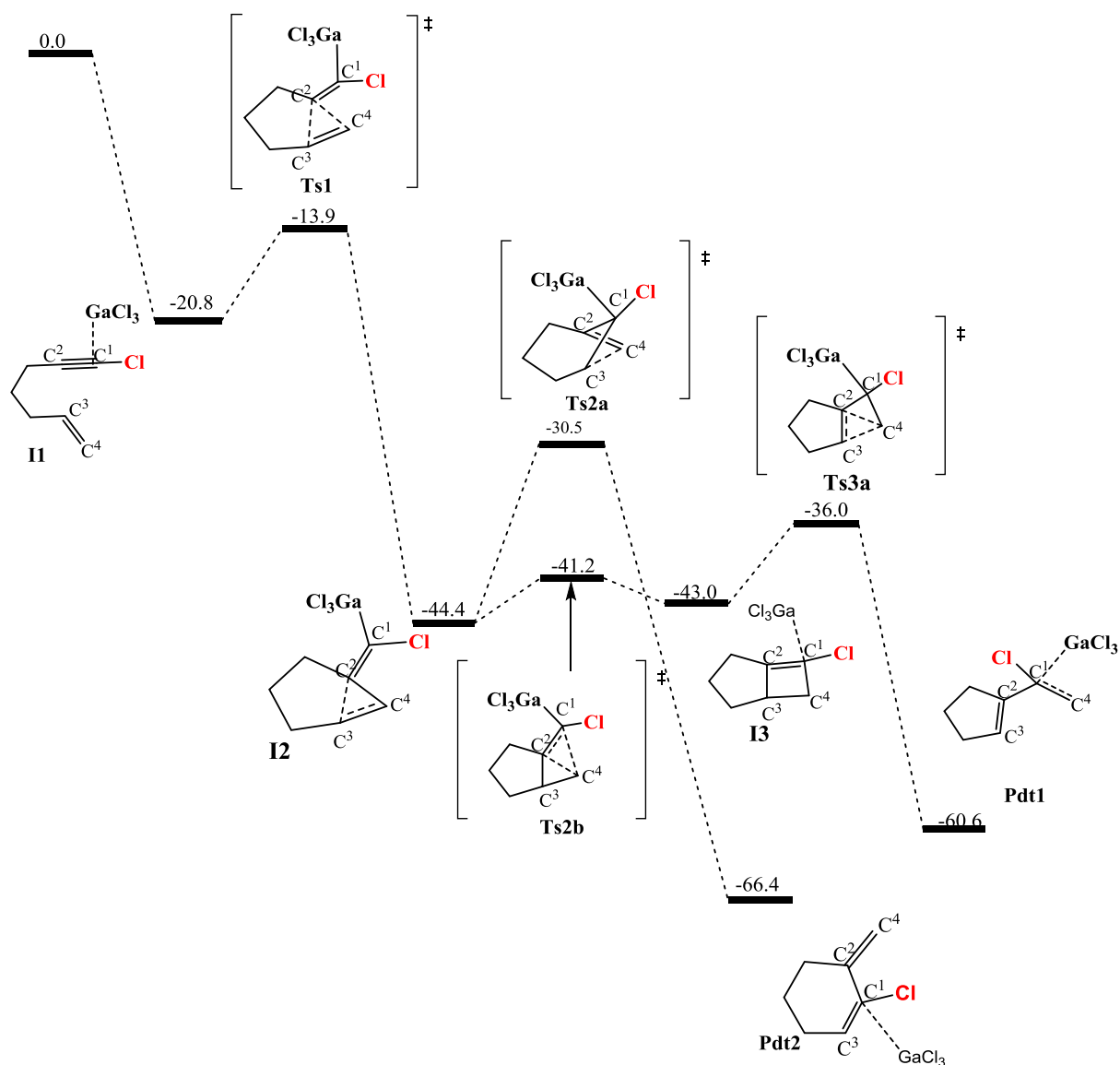


Fig. 4. Gibbs free energy profile of the skeletal reorganization of chlorine substituted enyne at the acetylenic moiety at the M06 level and 6-311G(d,p) basis set. Relative energies in kcalmol⁻¹.

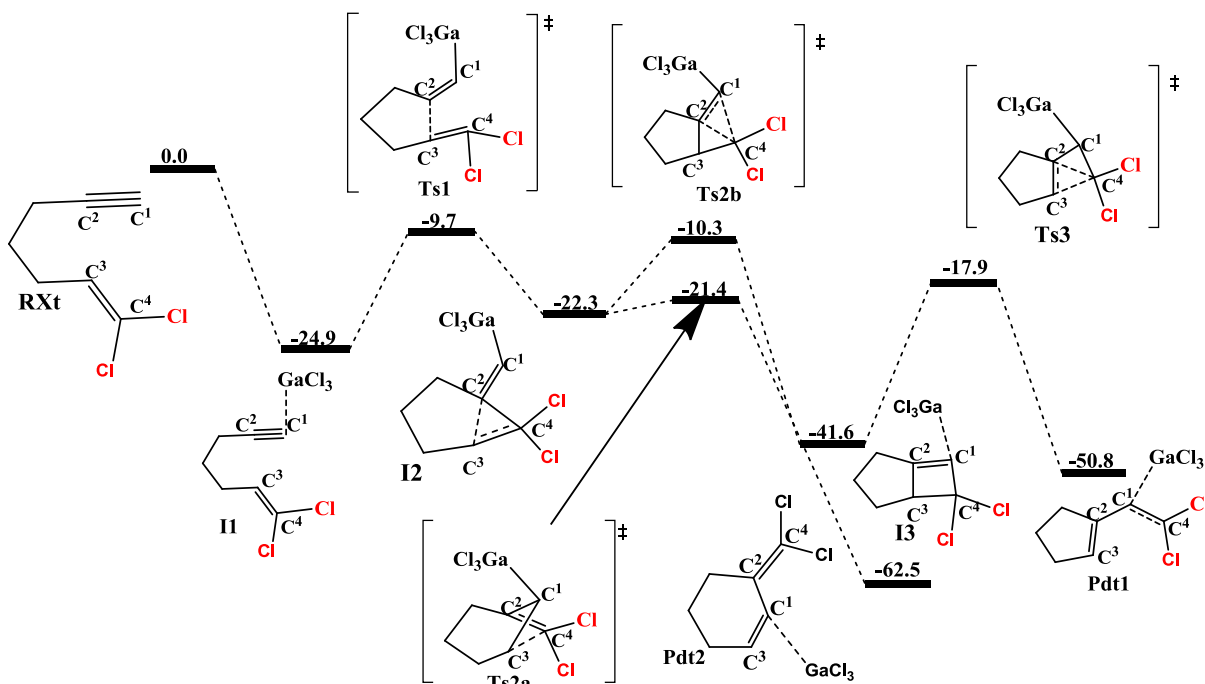


Fig. 5. Gibbs free energy profile of the skeletal reorganization showing the effect of di-substituted chlorine (EWG) enyne at the M06 level and 6-311G(d,p) basis set. Relative energies in kcalmol⁻¹.

Table 2

Relative energies of the stationary points on the potential energy surface, reaction energies and activation barriers for the di-substituted EWGs at the olefinic moiety. All energies are measured in kcal/mol.

Substituent	I1	Ts1a	I2	Ts2a	Ts2b	I3	Ts3a	Pdt1	Pdt2	Ea1	Ea2a	Ea2b	Ea3
H	-24.3	-14.3	-33.7	-29.9	-31.7	-47.3	-32.7	-60.6	-66.1	10.0	3.8	2.0	14.6
Cl	-24.9	-9.7	-22.3	-21.4	-10.3	-41.6	-17.9	-50.8	-62.5	15.2	0.9	12	23.7
CN	-22.9	-0.8	-13.2	-7.5	-5.4	-30.7	-10.0	-48.3	-60.6	22.1	6.0	8.1	20.7
CF ₃	-25.8	0.04	-18.6	-11.6	-11.0	-44.6	-12.5	-52.4	-47.0	25.8	7.0	7.6	32.1
NO ₂	-24.5	-0.3	-16.7	-4.7	-8.7	-41.7	-14.2	-58.4	-56.5	24.2	12.0	8.0	27.5

Ea1 is the first barrier leading to the formation of I2. Ea2a and Ea2b are the activation barrier leading to the formation of the Type III and I3 respectively. Ea3 is the last elementary step leading to formation of the Type I product.

for the -NH₂ substituted enyne, all the products formed have the metal weakly coordinated in the products. The substituents at the olefinic moiety can greatly alter the selectivity of the product. The elementary step leading to the formation of the type III product (I2a through TS2a to Type III) is disfavoured greatly when di-substituted EDGs or strong mono-substituted EDGs are employed. The transition state Ts2c and Ts3b leading to the formation of I3 and Type I occurs along the C1-C4 and C3-C4 respectively.

3.3. Substituent effect on the rate of Ga-Catalysed skeletal reorganization

In general, we observed that presence of the EWGs at the alkyne moiety favour the formation of Type I product kinetically (see Table 1 and Figs. S1-S3). The EWGs employed, -Cl, -CN, -NO₂, -COOCH₃ lowers the activation barriers Ea1 and Ea2b leading to I2 and I3. The lowering of Ts1a may be attributed to the electron withdrawing effect of the EWG which reinforces the electron

Table 3

Relative energies of the stationary points on the potential energy surface, reaction energies and activation barriers for the mono-substituted EWGs at the olefinic moiety. All energies are measured in kcal/mol.

R ¹ = EWG	I1	Ts1a	I2	Ts2a	Ts2b	I3	Ts3a	Pdt1	Pdt2	Ea1	Ea2a	Ea2b	Ea3
H	-24.3	-14.3	-33.7	-29.9	-31.7	-47.3	-32.7	-60.6	-66.1	10.0	3.8	2.0	14.6
Cl	-24.8	-11.7	-28.5	-25.2	-24.4	-43.4	-30.4	-54.4	-62.7	13.1	3.3	4.1	13.0
CN	-23.9	-5.7	-23.3	-17.8	-20.6	-39.1	-13.2	-53.6	-62.3	17.6	5.5	2.7	25.9
CF ₃	-24.8	-11.1	-28.1	-23.4	-23.3	-47.1	-30.7	-55.7	-62.7	13.7	4.7	4.8	16.4
NO ₂	-23.1	-6.2	-18.7	-15.3	-	-43.2	-17.7	-51.2	-55.0	16.9	3.4	-	25.5

Ea1 is the first barrier leading to the formation of I2. Ea2a and Ea2b are the activation barrier leading to the formation of the Type III and I3 respectively. Ea3 is the last elementary step leading to formation of the Type I product.

Table 4
Relative energies of the stationary points on the potential energy surface, reaction energies and activation barriers for the di-substituted EDGs at the olefinic moiety. All energies are measured in kcal/mol.

R ¹ = R ²	I1	Ts1c	I2	Ts2b*	I3	Ts3a*	Pdt1	Ea1	Ea2b	Ea3
H	-24.3	-14.3	-33.7	-31.7	-47.3	-32.7	-60.6	10.0	2.0	14.6
CH ₃	-25.7	-18.4	-31.3	-29.7	-42.0	-31.8	-64.3	7.3	1.6	10.2
Ph	-26.3	-20.0	-30.6	-27.3	-36.3	-23.1	-55.3	6.3	3.3	13.2
Pr	-26.5	-17.1	-31.5	-27.0	-44.4	-36.7	-63.1	9.4	4.5	8.0
OH	-29.3	-26.6	-41.9	-29.4	-40.4	-35.3	-79.3	3.0	12.5	5.1
NH ₂	-27.7	–	-58.3	-36.9	-39.2	-34.9	-89.5	–	21.4	4.3

Ea1 is the first barrier leading to the formation of I2. Ea2a and Ea2b are the activation barrier leading to the formation of the Type III and I3 respectively. Ea3 is the last elementary step leading to formation of the Type I product. For OH and NH₂, Ts2c and Ts3b occurred instead of Ts2b and Ts3a.

withdrawing effect of the GaCl₃, making the C2 carbon more electron deficient. This increases its affinity for the electron rich centre of the C3–C4 bond thereby shortening the bond length between C2–C3 and C2–C4. The **I1** complex formed easily transform through **Ts1a-cl** with an activation barrier of 6.9 kcal/mol to form **I2a-cl** when –Cl is employed compared to 10.0 kcal/mol in the parent enyne (Fig. 4). Transformation from **I2a** through **Ts2a** to form the Type III product is disfavoured by 10.7 kcal/mol compared

to 1.8 kcal/mol in the parent enyne. Formation of **I3** through the low barrier of 3.2 kcal/mol is therefore favoured. This trend is evident in all the EWGs reported thus far.

We extended this work by considering –Cl, –CN, –CF₃, –NO₂ mono and di-substituted enynes and their respective energy profiles are shown in Figs. S4–S9. Di-substituted weak EWGs tend to kinetically favour the formation of the type III product (Fig. 5). When –Cl di-substituted enyne was employed the transformation

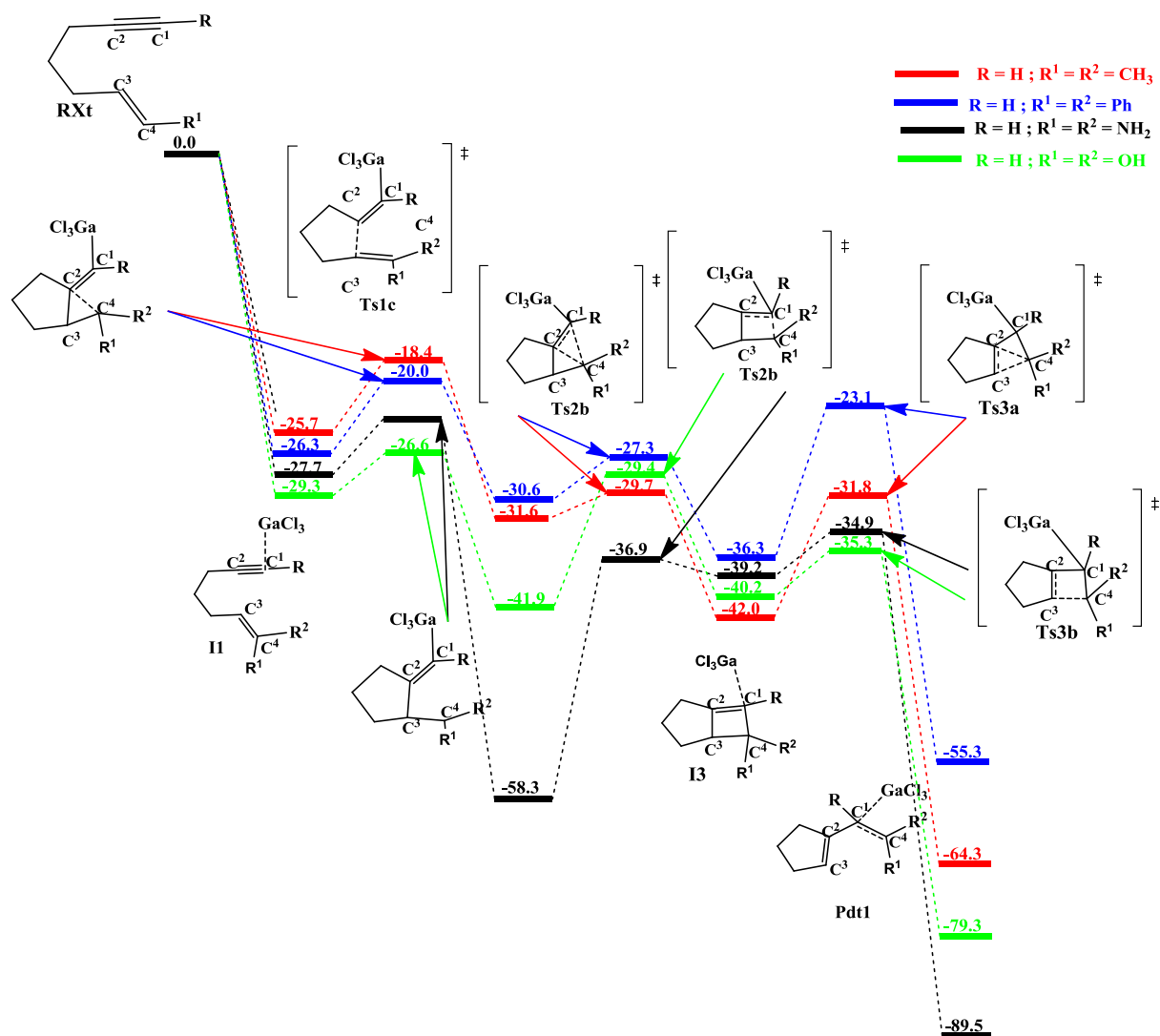


Fig. 6. Gibbs free energy profile of the skeletal reorganization of di-substituted EDGs at the olefinic moiety at the M06 level and 6-311G(d,p) basis set. Relative energies in kcalmol⁻¹. Di-substituted R = H, R¹ = R² = EDG.

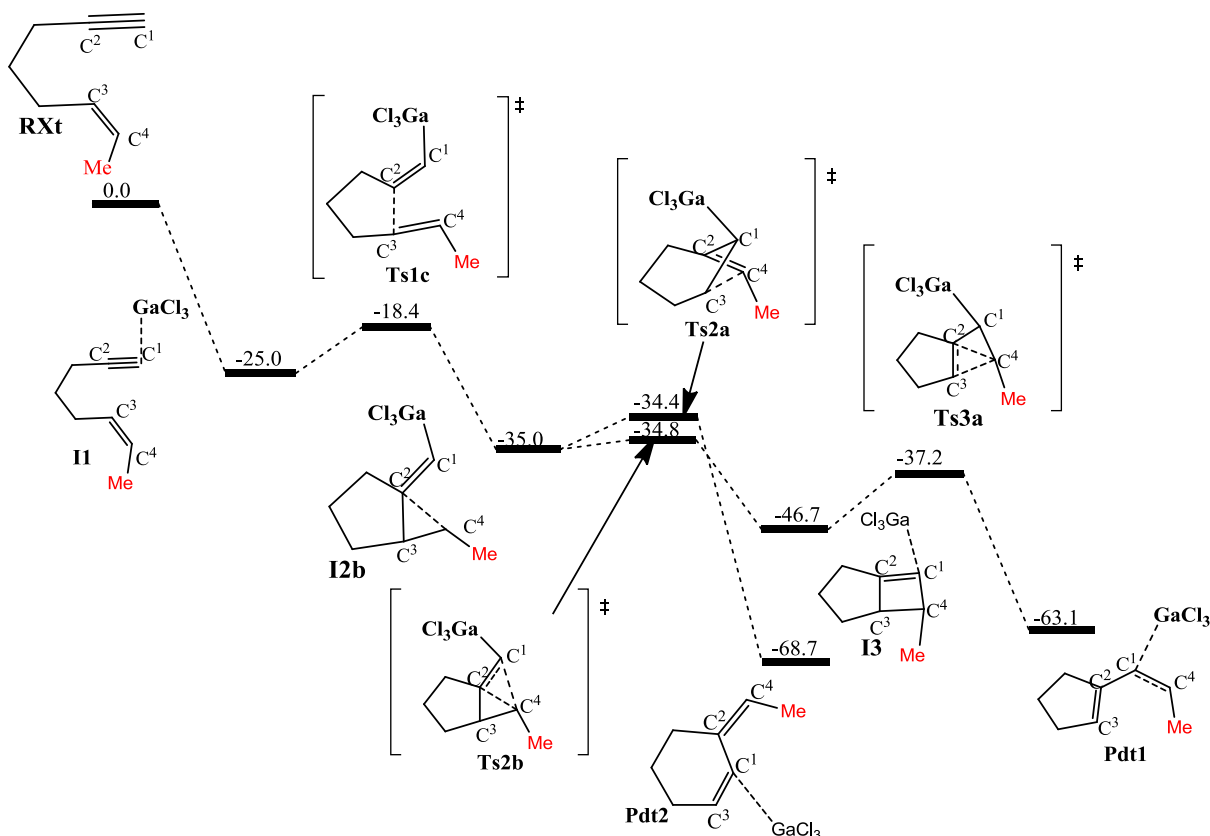


Fig. 7. Gibbs free energy profile of the skeletal reorganization methyl mono-substituted enyne at the M06 level and 6-311G(d,p) basis set. Relative energies in kcalmol⁻¹.

from **I2a** to the type **III** product went through an activation barrier of 0.9 kcal/mol compared to 12 kcal/mol leading to formation of **I3**. The elementary step leading to the formation of the Type **I** product is 23.7 kcal/mol compared to 14.6 kcal/mol in the parent enyne. In general all the di-substituted EWGs kinetically favour the Type **III** product except $-\text{NO}_2$ substituted as shown in Fig. S9 and Table 2. Even though mono-substituted EWGs (except $-\text{Cl}$ substituted) favoured the formation of the Type **I** product, the strong di substituted EDGs appear as a better alternative with a much lower activation barriers and can form Type **I** product at a higher yield (Tables 3 and 4).

In order to investigate the effect of EDGs on the formation of the type **I**, we employed mono- and di-substituted EDGs such as $-\text{CH}_3$, $-\text{Ph}$, $-\text{Pr}$, $-\text{NH}_2$, and $-\text{OH}$ (Table 4). We observed that in all, the substituents are oriented in the plane of the C3 – C4 bond. The di-substituted strong EDGs prove more efficient forming **I2c** totally reducing a possible formation of the type **III** product. The first activation barriers are lower compared to the parent enyne (Fig. 6).

Table 5

Relative energies of the stationary points on the potential energy surface, reaction energies and activation barriers for the mono-substituted EDGs at the olefinic moiety. All energies are measured in kcal/mol.

R ¹ = EDG	I1	Ts1c	I2	Ts2a	Ts2b*	I3	Ts3a*	Pdt1	Pdt2	Ea1	Ea2a	Ea2b	Ea3
H	-24.3	-14.3	-33.7	-29.9	-31.7	-47.3	-32.7	-60.6	-66.1	10.0	3.8	2.0	14.6
CH ₃	-25.0	-18.4	-35.0	-34.4	-34.8	-46.7	-37.2	-63.1	-68.7	6.6	0.6	0.2	9.5
Ph	-24.6	-19.0	-33.0	*	-32.4	-44.9	-38.5	-64.7	*	5.6	*	0.6	6.4
Pr	-25.1	-14.7	-37.4	-34.5	-34.9	-47.8	-37.6	-62.4	-66.3	10.4	2.9	2.4	10.2
OH	-26.1	-23.4	-30.9	*	–	-40.9	-30.3	*	-65.4	2.7	*	–	10.6
NH ₂	-26.3	-23.3	-50.2	*	-34.6	-41.9	-30.4	-75.7	*	3.0	*	15.9	11.5

Ea1 is the first barrier leading to the formation of **I2**. Ea2a and Ea2b are the activation barrier leading to the formation of the Type **III** and **I3** respectively. Ea3 is the last elementary step leading to formation of the Type **I** product. * The optimized geometry does not form under the specified substituent. For OH and NH₂ substituted, Ts2c and Ts3b occurred instead of Ts2b and Ts3a.

Di-substituted $-\text{CH}_3$, $-\text{Ph}$, $-\text{Pr}$, and $-\text{OH}$ went through **Ts1** with an activation barrier of 7.3, 6.3, 9.4, and 2.7 kcal/mol respectively compared to a barrier of 10.0 kcal/mol in the parent. Even though the activation barrier through **Ts2c** to form **I3** in $-\text{NH}_2$, $-\text{OH}$, is very high, about 21.4 and 12.5 kcal/mol respectively compared to 2.0 kcal/mol in the parent, the Type **III** pathway is totally eliminated and the Type **I** product forms exclusively. The alkyl groups $-\text{CH}_3$, and $-\text{Pr}$, is only slightly selective in the formation of the type **I** product (see Fig. 7). The propyl substituent shows much better selectivity of the type **I** over **III** product (see Table 5). This is consistent with the work done by Chatani et al. [8]. All the mono-substituted EDGs favour formation of the type **I** product. Selectivity of the type **I** product is increased when stronger EWGs are employed at the olefinic moiety. It is important to note here that only disubstituted olefins with R¹ = R² have been investigated in this study. If R¹ is different from R², additional pathways may exist leading to different products.

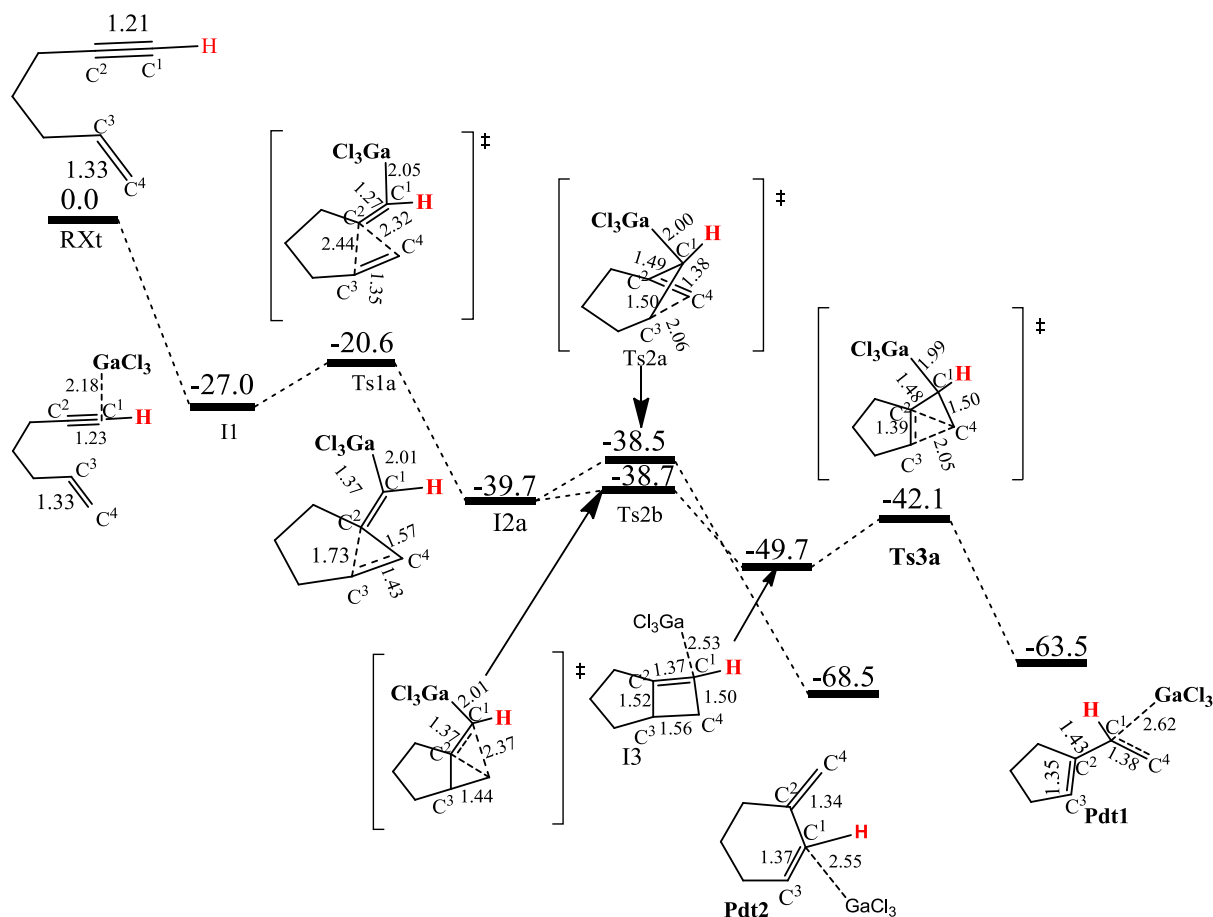


Fig. 8. Gibbs free energy profile of the skeletal reorganization of the parent enyne at the M06 level and 6-311G(d,p) basis set in toluene. Relative energies in kcalmol⁻¹. All bond distances are measured in Å.

3.4. Solvent effects on the energetics

Inspired by the fact that the original experimental work carried out on this subject by Chatani et al. [8], were done in toluene at 0 °C, we proceeded to investigate how the experimental conditions may affect the energetic trends. To this end, we repeated our DFT calculations on the GaCl₃-catalysed skeletal reorganization of the parent 1,6-enyne toluene at 298.15 K.

As evident in Fig. 8, changes in the magnitude of the energies for all the steps are obtained. However, the energetic trends and hence product distributions remain the same as that observed with the gas-phase calculations (Fig. 1). The optimized geometries of the reactants, transition states and intermediates involved in the skeletal reorganization of the parent enyne in toluene at 272.15 K and 298.15 K as well as the Gibbs free energy profile for the reaction are shown in Fig. 8. All the Cartesian coordinates and absolute energies relevant to this study are shown in table S1.

4. Conclusions

From the results discussed, the following conclusions are drawn:

- 1) The skeletal reorganization of enynes using GaCl₃ is very sensitive to the type of substituent at the olefinic and acetylenic moieties.
- 2) Substituents at the acetylenic moieties control the position of the metal along the alkyne bond. Unsubstituted and EWGs

substitution at the alkyne moiety have the metal sitting on the terminal carbon. EDGs allow the metal to sit on the internal carbon of the alkyne moiety. Therefore, the position of the metal in the pi-complex control the product formed.

- 3) Substituents at the olefinic moiety control selectivity of the product formed. EDG substituted enyne at the olefinic moiety selectively forms Type I. Strong di-substituted EDGs forms the Type I product exclusively. Weak di-substituted EWGs favour the formation of the type III product
- 4) The type I product is favoured when EWGs at the acetylenic moiety are employed as well strong di-substituted EDGs at the olefinic moiety. The type III product is formed selectively when weak di-substituted EWGs are employed.
- 5) It is established that solvent and temperature have negligible effects on the energetic trends and product distribution. Hence, gas-phase calculations are deemed adequate for the problem at hand.

Declaration of competing interest

The authors declare that there is no conflict of interests whatsoever regarding the publication of this manuscript.

Acknowledgements

The authors are very grateful to the National Council for Tertiary Education, Republic of Ghana, for a research grant under the Teaching and Learning Innovation Fund (TALIF/KNUST/3/0008/

2005), and to South Africa's Centre for High Performance Computing for access to additional computing resource on the Lengau cluster.

Appendix A. Supplementary data

Supplementary data to this article can be found online at <https://doi.org/10.1016/j.jmngm.2019.107476>.

References

- [1] C. Aubert, O. Buisine, M. Malacria, The behavior of 1,n-enynes in the presence of transition metals, *Chem. Rev.* (2002) 813–834, <https://doi.org/10.1021/CR980054F>.
- [2] B.M. Trost, Palladium-catalyzed cycloisomerizations of enynes and related reactions, *Acc. Chem. Res.* 23 (1990) 34–42, <https://doi.org/10.1021/ar00170a004>.
- [3] B.M. Trost, G.J. Tanoury, An unusual mechanism of a palladium-catalyzed intramolecular carbametalation. A novel palladium-catalyzed rearrangement, *J. Am. Chem. Soc.* 110 (1988) 1636–1638, <https://doi.org/10.1021/ja00213a054>.
- [4] C. Bruneau, Electrophilic activation and cycloisomerization of enynes: a new route to functional cyclopropanes, *Angew. Chem. Int. Ed.* 44 (2005) 2328–2334, <https://doi.org/10.1002/anie.200462568>.
- [5] K. Ota, S.I. Lee, J.-M. Tang, M. Takachi, H. Nakai, T. Morimoto, H. Sakurai, K. Kataoka, N. Chatani, Rh(II)-Catalyzed skeletal reorganization of 1,6- and 1,7-enynes through electrophilic activation of alkynes, *J. Am. Chem. Soc.* 131 (2009) 15203–15211, <https://doi.org/10.1021/ja9047637>.
- [6] N. Chatani, H. Inoue, T. Ikeda, S. Murai, Ru(II)- and Pt(II)-Catalyzed cycloisomerization of ω -Aryl-1-alkynes. Generation of carbocationic species from alkynes and transition metal halides and its interception by an aromatic ring, *J. Org. Chem.* 65 (16) (2000) 4913–4918, <https://doi.org/10.1021/jo000255v>.
- [7] C.H.M. Amijs, V. López-Carrillo, M. Raducan, P. Pérez-Galán, C. Ferrer, A.M. Echavarren, Gold(I)-Catalyzed intermolecular addition of carbon nucleophiles to 1,5- and 1,6-enynes, *J. Org. Chem.* 73 (2008) 7721–7730, <https://doi.org/10.1021/jo8014769>.
- [8] N. Chatani, H. Inoue, T. Kotsuma, S. Murai, Skeletal reorganization of enynes to 1-vinylcycloalkenes catalyzed by GaCl₃, *J. Am. Chem. Soc.* 124 (35) (2002) 10294–10295, <https://doi.org/10.1021/ja0274554>.
- [9] Y. M. N. Chatani, Skeletal Reorganization of Enynes Catalyzed by InCl₃, 2006, <https://doi.org/10.1021/OL060606D>.
- [10] T.J. Katz, T.M. Sivavec, Metal-catalyzed rearrangement of alkene-alkynes and the stereochemistry of metallacyclobutene ring opening, *J. Am. Chem. Soc.* 107 (1985) 737–738, <https://doi.org/10.1021/ja00289a054>.
- [11] A. Kinoshita, M. Mori, Total synthesis of (–)-Stemoamide using ruthenium-catalyzed enyne metathesis reaction, *J. Org. Chem.* 61 (1996) 8356–8357, <https://doi.org/10.1021/jo9616872>.
- [12] Atsushi Kinoshita, Norikazu Sakakibara, M. Mori, Novel 1,3-diene synthesis from alkyne and ethylene by ruthenium-catalyzed enyne metathesis, *J. Am. Chem. Soc.* 119 (50) (1997) 12388–12389, <https://doi.org/10.1021/JA973134U>.
- [13] L.-G. Zhuo, J.-J. Zhang, Z.-X. Yu, DFT and experimental exploration of the mechanism of InCl₃-catalyzed type II cycloisomerization of 1,6-enynes: identifying InCl₂⁺ as the catalytic species and answering why nonconjugated dienes are generated, *J. Org. Chem.* 77 (2012) 8527–8540, <https://doi.org/10.1021/jo301471w>.
- [14] L.-G. Zhuo, J.-J. Zhang, Z.-X. Yu, Mechanisms of the InCl₃-catalyzed type-I, II, and III cycloisomerizations of 1,6-enynes, *J. Org. Chem.* 79 (2014) 3809–3820, <https://doi.org/10.1021/jo5000059j>.
- [15] V. Michelet, P.Y. Toullec, J.-P. Genêt, Cycloisomerization of 1,n-enynes: challenging metal-catalyzed rearrangements and mechanistic insights, *Angew. Chem. Int. Ed.* 47 (2008) 4268–4315, <https://doi.org/10.1002/anie.200701589>.
- [16] Hiroki Inoue, Naoto Chatani, S. Murai, Cycloisomerization of ω -Aryl-1-alkynes: GaCl₃ as a highly electrophilic catalyst for alkyne activation, *J. Org. Chem.* 67 (4) (2002) 1414–1417, <https://doi.org/10.1021/jo016232d>.
- [17] K. Xu, Y. Wu, D. Xie, G. Yan, Mechanism of skeletal reorganization of 1,6-enynes catalyzed by GaCl₃, *Chinese Sci. Bull. (Arch. Am. Art)* 49 (2004) 883–885, <https://doi.org/10.1007/BF03184003>.
- [18] V. Verdolino, A. Forbes, P. Helquist, O. Wiest, On the mechanism of the rhodium catalyzed acrylamide hydrogenation, *J. Mol. Catal. A Chem.* 324 (2010) 9–14, <https://doi.org/10.1016/j.molcata.2010.02.026>.
- [19] M.S.G. Ahlquist, Iridium catalyzed hydrogenation of CO₂ under basic conditions—mechanistic insight from theory, *J. Mol. Catal. A Chem.* 324 (2010) 3–8, <https://doi.org/10.1016/j.molcata.2010.02.018>.
- [20] C.L. McMullin, B. Rühle, M. Besora, A.G. Orpen, J.N. Harvey, N. Fey, Computational study of PtBu₃ as ligand in the palladium-catalyzed amination of phenylbromide with morpholine, *J. Mol. Catal. A Chem.* 324 (2010) 48–55, <https://doi.org/10.1016/j.molcata.2010.02.030>.
- [21] Wavefunction, Spartan 14' v.1.1.8, Wavefunction, 2014.
- [22] M.J. Frisch, G.W. Trucks, H.B. Schlegel, G.E. Scuseria, M.A. Robb, J.R. Cheeseman, G. Scalmani, V. Barone, B. Mennucci, G.A. Petersson, H. Nakatsuji, M. Caricato, X. Li, H.P. Hratchian, A.F. Izmaylov, J. Bloino, G. Zheng, J.L. Sonnenberg, M. Hada, M. Ehara, K. Toyota, R. Fukuda, J. Hasegawa, M. Ishida, T. Nakajima, Y. Honda, O. Kitao, H. Nakai, T. Vreven, J.A. Montgomery, J.E. Peralta, F. Ogliaro, M. Bearpark, J.J. Heyd, E. Brothers, K.N. Kudin, V.N. Staroverov, R. Kobayashi, J. Normand, K. Raghavachari, A. Rendell, J.C. Burant, S.S. Iyengar, J. Tomasi, M. Cossi, N. Rega, J.M. Millam, M. Klene, J.E. Knox, J.B. Cross, V. Bakken, C. Adamo, J. Jaramillo, R. Gomperts, R.E. Stratmann, O. Yazyev, A.J. Austin, R. Cammi, C. Pomelli, J.W. Ochterski, R.L. Martin, K. Morokuma, V.G. Zakrzewski, G.A. Voth, P. Salvador, J.J. Dannenberg, S. Dapprich, A.D. Daniels, Ö. Farkas, J.B. Foresman, J.V. Ortiz, J. Cioslowski, D.J. Fox, Gaussian 09, Revision B. 01, Gaussian Inc., Wallingford, CT, 2009, p. 6492.
- [23] Y. Zhao, D.G. Truhlar, Density functionals with broad applicability in chemistry, *Acc. Chem. Res.* 41 (2008) 157–167, <https://doi.org/10.1021/ar700111a>.
- [24] S.N. Pieniazek, F.R. Clemente, K.N. Houk, Sources of error in DFT computations of C–C bond formation thermochemistries: $\pi \rightarrow \sigma$ transformations and error cancellation by DFT methods, *Angew. Chem. Int. Ed.* 47 (2008) 7746–7749, <https://doi.org/10.1002/anie.200801843>.
- [25] J. Tomasi, B. Mennucci, R. Cammi, Quantum mechanical continuum solvation models, *Chem. Rev.* 105 (2005) 2999–3093, <https://doi.org/10.1021/cr9904009>.
- [26] M. Clark, R.D. Cramer, N. Van Opdenbosch, Validation of the general purpose tripos 5.2 force field, *J. Comput. Chem.* 10 (1989) 982–1012, <https://doi.org/10.1002/jcc.540100804>.
- [27] E. Opoku, R. Tia, E. Adei, DFT mechanistic study on tandem sequential [4 + 2]/[3 + 2] addition reaction of cyclooctatetraene with functionalized acetylenes and nitrile imines, *J. Phys. Org. Chem.* (2019), e3992, <https://doi.org/10.1002/poc.3992>.
- [28] E. Opoku, R. Tia, E. Adei, [3 + 2] versus [2 + 2] Addition: a density functional theory study on the mechanistic aspects of transition metal-assisted formation of 1,2-dinitrosoalkanes, *J. Chem.* 2016 (2016) 10, <https://doi.org/10.1155/2016/4538696>.
- [29] E. Opoku, R. Tia, E. Adei, Computational studies on [4 + 2]/[3 + 2] tandem sequential cycloaddition reactions of functionalized acetylenes with cyclopentadiene and diazoalkane for the formation of norbornene pyrazolines, *J. Mol. Model.* 25 (2019) 168, <https://doi.org/10.1007/s00894-019-4056-x>.
- [30] E. Opoku, R. Tia, E. Adei, Quantum chemical studies on the mechanistic aspects of tandem sequential cycloaddition reactions of cyclooctatetraene with ester and nitrones, *J. Mol. Graph. Model.* 92 (2019) 17–31, <https://doi.org/10.1016/j.jmngm.2019.06.019>.
- [31] G. Arhin, A.H. Adams, E. Opoku, R. Tia, E. Adei, 1,3-Dipolar cycloaddition reactions of selected 1,3-dipoles with 7-isopropylidenebornadiene and follow-up thermolytic cleavage: a computational study, *J. Mol. Graph. Model.* 92 (2019) 267–279, <https://doi.org/10.1016/j.jmngm.2019.08.004>.
- [32] D. Roland, J.N. Haleegoah, E. Opoku, R. Tia, E. Adei, Mechanistic studies on tandem cascade [4 + 2]/[3 + 2] cycloaddition of 1,3,4-oxadiazoles with olefins, *J. Mol. Graph. Model.* 93 (2019) 107452, <https://doi.org/10.1016/j.jmngm.2019.107452>.
- [33] K.N. Kudin, G.E. Scuseria, E. Cancès, A black-box self-consistent field convergence algorithm: one step closer, *J. Chem. Phys.* 116 (2002) 8255, <https://doi.org/10.1063/1.1470195>.
- [34] C.E. Dykstra, *Theory and Applications of Computational Chemistry: the First Forty Years*, first ed., Elsevier, Amsterdam; Boston, 2005.